Sample Holders for Sub-THz Electron Spin Resonance Spectroscopy

Antonín Sojka, Matúš Šedivý, Adam Lagiň, Andrej Gabriš, Tomáš Láznička, Vinicius Tadeu Santana, Oleksii Laguta, and Petr Neugebauer

***Abstract*— Electron spin resonance (ESR) is a powerful spectroscopic technique used to investigate samples with unpaired electrons in a broad range of scientific fields. High-frequency ESR (HF-ESR) spectrometers operating at sub-THz frequencies are mostly custom-made with non-standard solutions. This article presents a set of six different exchangeable sample holders with a fast-loading flange for a sub-THz ESR spectrometer operating at high magnetic fields up to 16 T and temperature ranges of 4–400 K. Here, we report on the concept, design, and illustrative measurements of non-resonant ESR sample holders for the measurements of samples in a liquid solution, polycrystalline-compressed powders, oriented single crystals, electrical devices under sub-THz irradiation, as well as for samples transferred from the ultrahigh vacuum (UHV) systems without air contamination. Our solution expands the usage possibilities for HF-ESR spectroscopy, showing that one spectrometer with the presented concept of sample holders enables a wide range of applications.**

***Index Terms*— Frequency-domain magnetic resonance (FDMR), high-field/high-frequency electron spin resonance (ESR)/EPR, high-frequency (HF) EPR, liquids, rapid scan (RS) ESR, single-crystal, ultrahigh vacuum (UHV).**

I. Introduction

SINCE the discovery of electron spin resonance (ESR) by Zavoisky in 1944 at Kazan Federal University, Kazan, Russia [1], there has been vast development in the field of magnetic resonance. Nowadays, ESR methodologies cover various science disciplines [2], including solid-state physics [3]–[7], quantum information processing [8], [9], biophysics [10]–[14], and chemistry [15]–[17].

The principle of ESR is based on the Zeeman effect (see Fig. 1), where the magnetic component, B_1, of an electromagnetic wave at frequency f interacts with the magnetic moment of an unpaired electron spin, $S = 1/2$, in the presence of an applied external magnetic field B_0. The resonance condition for $S = 1/2$ is then as follows:

$$\Delta E = E_1 - E_2 = hf = g\mu_B B_{\text{res}} \tag{1}$$

where E_1 and E_2 are energies of the two possible m_s states of spin $S = 1/2$, h is the Planck constant, B_{res} is the resonance field, and g is the g-factor, a fingerprint of the measured atom, molecule, or structure containing the unpaired electron. For a free (unbound) electron, $g = g_e = 2.00231930436146(56)$ [18], one of the most precisely measured nature constants. The resonance condition implies that the irradiation frequency ratio to the magnetic field scales as 28 GHz/T, comprising the microwave (MW) range.

An absorption ESR signal is observed when the resonance condition is fulfilled, for example, when the electromagnetic wave's energy hf matches the energy levels' separation ΔE (see Fig. 1). In order to further improve the ESR signal-to-noise ratio (SNR), a small modulating field, B_{mod}, oscillating at a few kHz, is applied, leading to the actual measurement of the derivative of an absorption spectra (see Fig. 1) [19]. In the case of a system with more than one unpaired electron, $S > 1/2$, the spin–spin and spin–orbit couplings may lift the degeneracy of spin states even at zero-field, the so-called zero-field splitting (ZFS). This is often the case of important molecules for technical developments in the field of quantum computing and data storage [20], [21], the so-called single-molecule magnets (SMMs) or single-ion magnets (SIMs). SMMs or SIMs are based either on the transition metals (Mn, Fe, Co, etc. [22]–[25]) or lanthanides [26], [27]. In these cases, a typical ESR spectrometer operating at X-band frequencies (9.6 GHz, 0.343 T for $g = 2$) is not able to access ZFS transitions [5], [28]. This limitation drove research efforts to develop ESR spectrometers at higher frequencies, enabling access to these higher energy transitions and to improved sensitivity and enhanced spectral resolution [26], [29]–[32].

The advances in MW technologies have been driving the development of new methodologies in ESR [33], resulting in the commercially available ESR spectrometers operating at J-band frequencies (263 GHz, 9.395 T for $g = 2$) (Bruker Corporation, Billerica, USA) and custom-made spectrometers working in a broad range of frequencies up to the THz range [34], [35]. These ESR spectrometers work either in a pulsed or in a continuous wave (CW) regime. Whereas high-frequency CW-ESR spectrometers operate at low MW

Manuscript received January 6, 2022; revised March 10, 2022; accepted March 18, 2022. Date of publication April 1, 2022; date of current version April 19, 2022. The work of Antonín Sojka, Andrej Gabriš, and Vinicius Tadeu Santana was supported by the European Research Council (ERC) through the European Union's Horizon 2020 Research and Innovation Program under Grant 714850. The work of Matúš Šedivý, Oleksii Laguta, and Petr Neugebauer was supported by the Grant Agency of the Czech Republic under Grant EXPRO: 21-20716X. The work of Adam Lagiň and Tomáš Láznička was supported by the Ministry of Education, Youth and Sports of the Czech Republic under the INTER-EXCELLENCE Program under Grant LTAUSA19060. The Associate Editor coordinating the review process was Dr. Tae-Weon Kang. *(Corresponding author: Petr Neugebauer.)*

The authors are with the Central European Institute of Technology, Brno University of Technology, 61200 Brno, Czech Republic (e-mail: antonin.sojka@ceitec.vutbr.cz; petr.neugebauer@ceitec.vutbr.cz).

This article has supplementary downloadable material available at https://doi.org/10.1109/TIM.2022.3164135, provided by the authors.

Digital Object Identifier 10.1109/TIM.2022.3164135

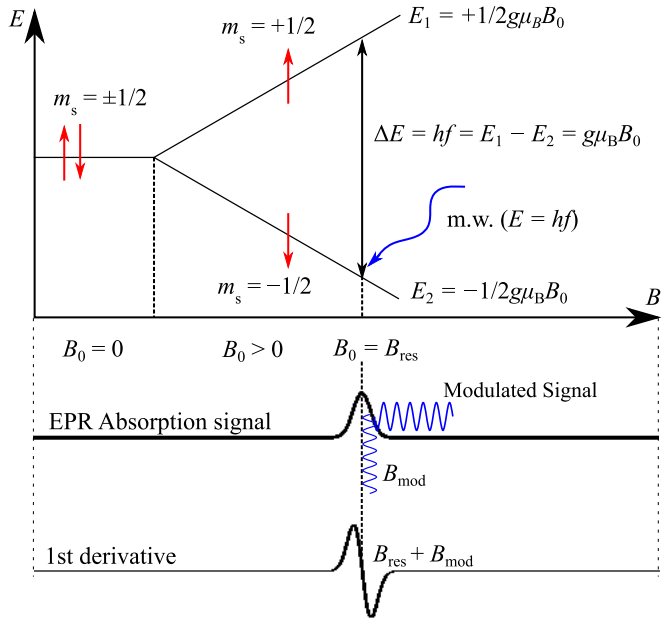

Fig. 1. Illustration showing an interaction of an electron spin, $S = 1/2$, with an external magnetic field, $\boldsymbol{B}_0$, and an oscillating electromagnetic irradiation at frequency f (microwave range, GHz). If the magnitude of the external magnetic field B_0 is zero, there is no energy difference between the two spin states $m_S = +1/2$ and $m_S = -1/2$, and they are degenerated. In the presence of the external magnetic field ($B_0 \neq 0$), the degeneracy is lifted and the two states E_1 and E_2 are separated by ΔE, the Zeeman splitting. By applying an appropriate microwave at energy $hf = \Delta E$ matching the Zeeman splitting, an ESR absorption signal is observed. In the typical ESR experiment, the lock-in technique is used, the weak ESR absorption signal is encoded by a small modulation of the external magnetic field B_{mod} by a modulation coil at the frequency of a few kHz, which results in observing the first derivative of the absorption ESR signal.

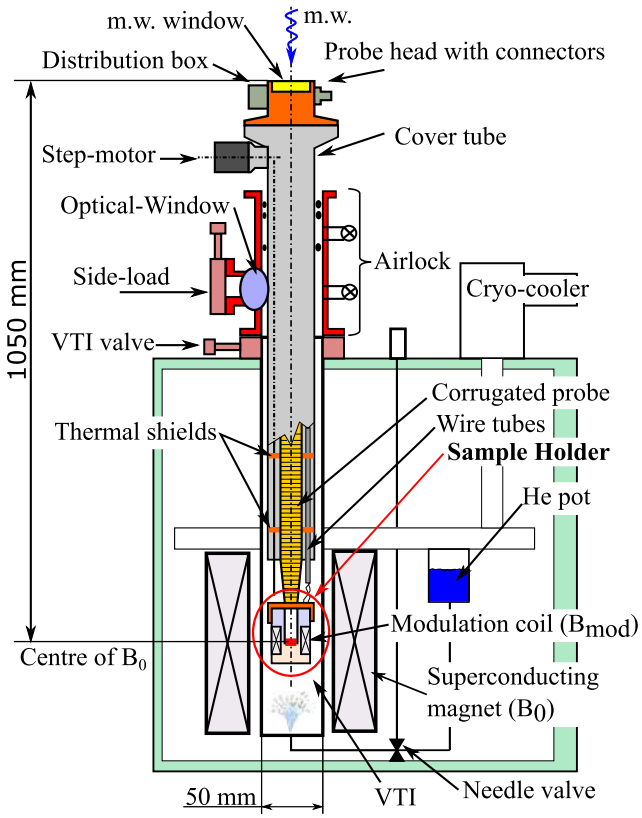

Fig. 2. Schematic drawing of the ESR probe with an SH located in a cryogen-free superconducting magnet equipped with a variable temperature insert (VTI).

power (typically few milliwatts) using non-resonant sample holders allowing multi-frequency ESR [36], the pulsed-ESR spectrometers need high-power microwaves on the sample and use resonant cavities in order to flip magnetization [19], which restricts the operation to single-frequency excitation only with a narrow bandwidth (less than 1 GHz). Besides obtaining the ESR spectra, the pulsed ESR spectrometers also provide information about the spin dynamics [19]. Historically, both mentioned methods are performed in the field domain due to the easy sweep of the magnetic field when compared to sweeping an excitation frequency. However, the recent development of microwave technologies has enabled frequency-domain magnetic resonance (FDMR) spectroscopy with high sensitivity [29], [34], [37]–[39]. Many HF-ESR groups have previously described systems including different types of sample holders [34], [36], [40]–[43].

FDMR spectrometers in combination with non-resonant sample holders allows the performance of rapid scan (RS) ESR [30], [44], [45]. If the frequency is swept through the resonance faster than the relaxation times of the sample, the recorded signal is in the form of "wiggles" containing information on the spin dynamics. The deconvolution of the RS signal removes these wiggles, giving a non-distorted ESR absorption spectrum, and the relaxation time T_2 can be obtained with the help of the modified Bloch equations [46]. The main advantages of RS over pulse ESR are much broader operating range (tens of GHz) and the absence of a dead time (in which the detector is protected from the MW source's high power). Therefore, RS can theoretically measure extremely short T_2 (ns) relaxation times at any frequency within the spectrometer's frequency range [30], [47].

ESR has broad applications ranging from physics, over chemistry to biology, and therefore a wide variety of sample types exist with different requirements [2], [48]. The message of this article is to show that any spectrometer using a sample holder without a resonator (non-resonant sample holder) has a wide range of applications, which can be reached by designing new sample holders. Therefore, here we report on the concept, design, and production of six different exchangeable non-resonant ESR sample holders (SHs): a simple sample holder (SSH) for measuring pressed-powder pellets; a rotator sample holder (RSH) for recording the ESR spectra of a crystal with magnetic anisotropy; a chip sample holder (ChSH) for measuring and testing nanodevices under MW irradiation; a liquid sample holder (LSH) for measuring samples in liquid form and air-sensitive samples; a carousel sample holder (CSH) for loading up to six pressed-powder pellets to significantly save the spectrometer time, and finally, a vacuum sample holder (VSH), which is designed for measurements of samples transferred from UHV systems without air contamination.

II. Experimental Setup

The SHs are designed for a sub-THz frequency rapid scan (FRaSCAN) ESR spectrometer. Fig. 2 depicts schematic

part of the FRaSCAN ESR spectrometer where SHs are placed. The SHs are located at the end of the measurement probe (about 1-m long) that is inserted into a cryogen-free superconducting solenoid magnet equipped with a variable temperature insert (VTI) with 50 mm of diameter sample space (Cryogenics Ltd., London, U.K.). A home-built airlock port is used for the probe insertion to avoid contamination of the closed-cycle helium environment by pumping and flushing the probe space before it slides into the operation position through the then opened VTI valve. Moreover, the airlock has a port for side-loading samples that can be transferred from a glove box or UHV system with an optical window to allow the visual check of the sample is being loaded into the dedicated VSH. The sample in an SH is at the end of a corrugated MW waveguide. Two corrugated waveguides (Thomas Keating Ltd., Billingshurst, U.K.) were manufactured from German silver, one designed for 100 GHz and the other for 430 GHz. The waveguide is placed inside a non-magnetic stainless steel cover (cover tube) and centered by sets of thermal shields along the waveguide. At the top of the probe, the MW corrugated waveguide is attached to the head, which contains three electrical connectors—DBEE104A056, SFE104A086, and SFE102A053 (Fischer Connectors, Saint-Prex, Switzerland)—and one custom-built optical connector. The uniqueness of each connector prevents them from being changed unintentionally. The MW window in the head is a 2.213-mm-thick high-density polyethylene (HDPE) film. The electrical wires (see supplementary information) are shielded and guided in two stainless steel tubes to a fast loading flange (FLF), where the SHs are attached. The first tube carries wires for custom-made modulation coils, temperature sensors (T-sensor) Cernox CX 1050 HT (LakeShore Cryotronics Inc., Westerville, USA), and optional heaters and field sensors, whereas the second tube guides wires for sensitive electrical measurements. The MW used to irradiate the sample in the center of the magnetic field is generated outside the VTI by a synthesizer (8–14 GHz) and multiplied by a set of frequency multipliers and amplifier–multiplier chains (AMCs) (all from Virginia Diodes Inc., Charlottesville, USA) into the desirable frequency in a range of 90–1100 GHz.

Then, the MW is focused with outside-located optics (not shown) through the HDPE window into the oversized corrugated waveguide with an inner diameter of 18 mm and propagates there with minimal losses to the inlet MW port of an SH. There, using a focusing corrugated taper, the MW is focused from 18-mm down to 5-mm diameter into the SH waveguide. The MW waveguide is used to guide also the reflected MW from a sample back to the outside optics. Furthermore, the cover tube is equipped with a port for a piezo step-motor (PiezoMotor Uppsala AB, Uppsala, Sweden), which is used to rotate a shaft used in the CSH. The shaft goes down along the corrugated waveguide to the FLF.

III. Sample Holder Features

Reproducible, fast, and user-friendly exchange of SHs is very desirable for any measurement system, not only for HF-ESR spectroscopy. It speeds up the setting of a typical experiment and prevents user errors, that is, bad wiring or misalignment, which may affect the reproducibility of the experiment and waste expensive measurement time. For this reason, we developed a set of SHs compatible with the FLF (see Fig. 3). All parts of the SHs need to withstand an operating temperature between 4 and 400 K with negligible volume change to keep the MW alignment and thus ensure good MW coupling with the samples. Additionally, they have to be non-magnetic and preferably non-metallic in order to provide sufficiently large field modulation (B_{mod}) on a sample and to prevent the generation of eddy currents. For these reasons, we found poly-ether ether ketone (PEEK) to be an optimal material, and most parts of the SH are fabricated with it. PEEK withstands the large thermal cycling required in ESR experiments and is easily machinable, with a good mechanical stability [49].

The design of different SHs can be split into two main categories: bottom-load and side-load SHs. The bottom-load SHs are easier to manufacture, thanks to their cylindrical symmetry, have a modulation coil in a solenoid shape, and provide an optimal MW alignment during the screwing of the functional part into the body. The side-load SHs use Helmholtz modulation coils and possess an extra level of complexity that allows insertion via a side-load port on the airlock in the case of air-sensitive samples, or allow inserting multiple samples which can be loaded at once into the VTI. Both categories are designed to have a maximal outer diameter of 42 mm and can be split into three parts (see Fig. 3): 1) the FLF that redistributes all the necessary contacts and is attached to the end of the corrugated waveguide; 2) a body docked by four aluminum pins to the FLF with electrical connectors and that contains a modulation coil and a smooth MW waveguide; and 3) a functional part that contains the sample and is inserted into the body. All parts are described in the following text in greater detail.

A. Fast Loading Flange (FLF)

The design of the FLF consists of two main parts: a rotary and a base part (see Fig. 3). The rotary part is free to rotate in a given range on the base part and it has four grooves for the locking pins, one of which is larger to ensure a single coupling position for the SH. The base part is connected directly to the end of the corrugated waveguide. It has 24 female contacts CPINM-10 (LewVac, Burgess Hill, U.K.) divided into three connector blocks and a hole for a shaft connection. The rotary part rotates 90° around the axis of the waveguide, pushing the SH body and locking pins into the flange. Also upon rotation, all required contacts CPINM-10 are fastened to the female connectors grouped into three custom-made insulated eight-connector blocks. For good electric insulation and stability, the connector blocks are made from PEEK. The central eight-connector block contains electric contacts that are the same for all SHs: two for modulation coils, two for the T-sensor (Cernox CX 1050 HT, LakeShore Cryotronics Inc., USA), and four auxiliary ones can be used, for instance, for a magnetic field sensor (HGA-2302, LakeShore Cryotronics Inc., USA) or additional heater if needed. The other lateral eight-connector blocks contain connectors for RSH, CSH, and ChSH.

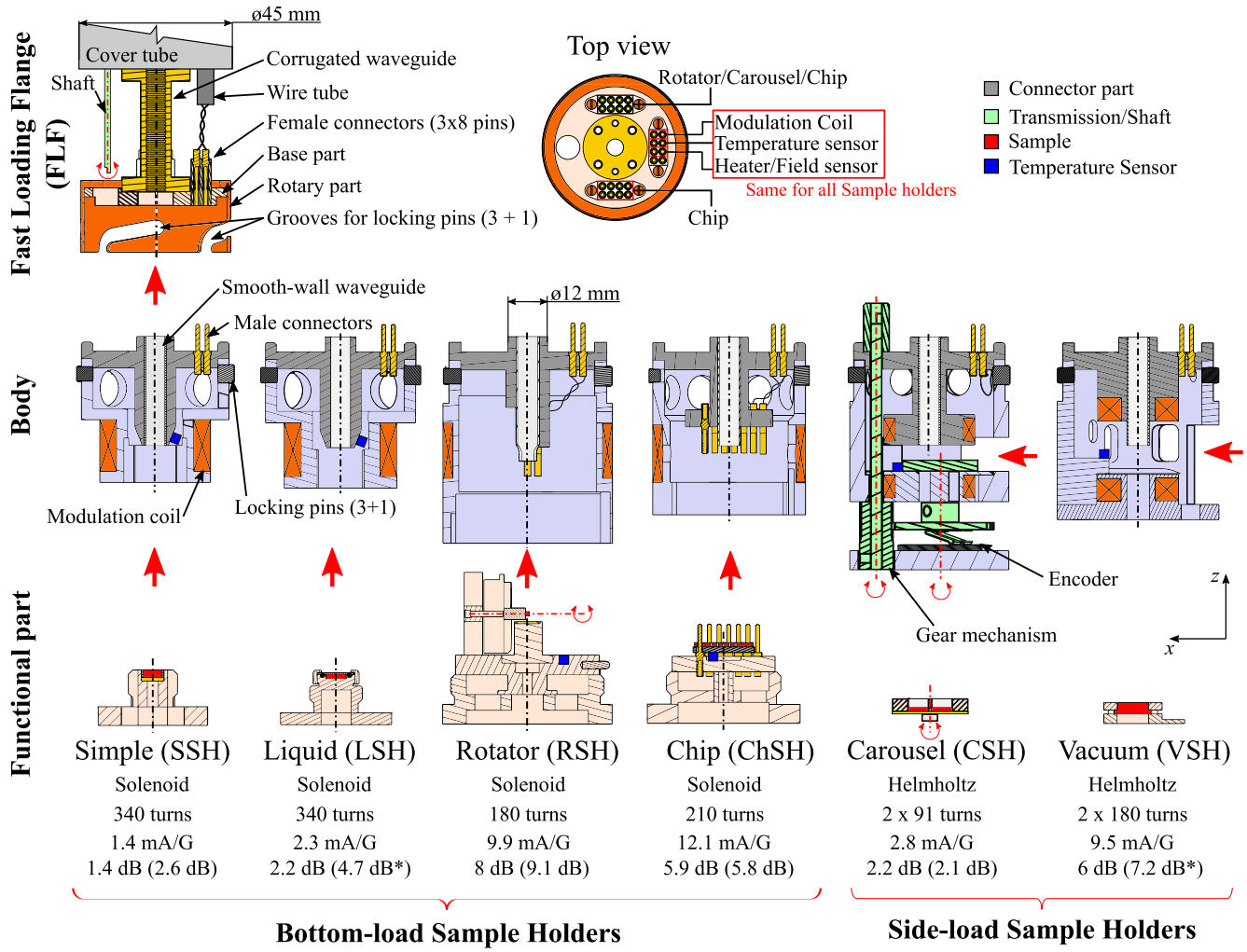

Fig. 3. Schematic picture of the sample holders' concept. The SHs can be divided into three parts: the FLF attached to the end of the corrugated MW waveguide, the body of SHs, and the functional parts, where the samples are located. All functional parts with their respective bodies are compatible with the FLF. The FLF consists of a set of three eight-connector blocks linked by wires to the probe head connectors, a rotary part with grooves for locking pins at bodies, and a shaft used in combination with a step-motor to exchange the sample in the CSH. During loading of bodies into the FLF, all electrical contacts and MW alignment is made smoothly during the sliding of the locking pins into the grooves by rotating the rotary part of the flange. Furthermore, the bodies can be divided into two groups: Bottom-load SH and Side-load SH with solenoid and Helmholtz modulation coils, respectively. The Bottom-load SHs have a functional part with a sample screwed into the body, whereas the Side-load SHs have a sample placed on the platform inserted from the side. The functional parts with the location of the SHs are also shown and are described in great detail in Figs. 4–9. Additional parameters of the modulation coils are listed, including the number of turns, the current for creating 1 Gauss at 1-kHz modulation, the MW attenuation at 430 GHz, and the average of MW attenuation of the assembled SHs measured in the frequency range (260–500) GHz or (325–500)* GHz.

The rotary part of the flange is made from brass, whereas the base part is made from PEEK to provide thermal insulation of the SH from the corrugated waveguide, resulting in better thermal control of the sample. Experimentally, we observe that this solution decreases the cooling time of the SH from 300 to 4 K to 6 h, which is a one-third less time when compared to the situation where the base part is made from brass.

B. Body of Sample Holders

The body of SHs is made of PEEK with four aluminum pins to fit into FLF grooves and several holes to allow effective helium cooling. The body contains a modulation coil, a smooth-walled MW waveguide, and a connector part. As mentioned, we divide the SHs for bottom- and side-loading type, with solenoid or Helmholtz modulation coils, respectively. The parameters of the modulation coils were simulated via the COMSOL Multiphysics software (see supplementary information). Furthermore, the precise field modulation amplitude was measured experimentally by overmodulating the ESR spectrum on a reference sample of lithium phthalocyanine (LiPc). The current values obtained to create 1 Gauss modulation at 1-kHz frequency are listed at the bottom of Fig. 3, including the type of coil and number of turns. The coils were wided from Cu 32 AWG wire (LakeShore Cryotronics Inc., USA). Additional information on modulation can be found in the supplementary information.

A smooth-walled MW waveguide of aluminum has an inner diameter of 5 mm, with a wall thickness of 0.5 mm. It is pressed into the PEEK connector part of the body and aligned at the FLF by a rim with a diameter of 12 mm to ensure

proper MW coupling. The length of the waveguide varies from body to body and in the case of Rotator SH, it has a cutout for entering a sapphire rod with a sample at the bottom end.

All SH bodies contain all necessary wire connections; therefore, there is no need for further interaction from the user besides the placement of a sample on a functional part. In the case of simple, liquid, carousel, and vacuum SHs, SH body also contains a T-sensor; only in the case of rotator and chip SH, the el. connections are further transferred from the bodies to functional parts.

C. Functional Parts of Sample Holders

All functional parts are designed to enable visual and manipulation access to the sample, helping with its alignment and visual check outside of the SH body (e.g., by an optical microscope). If not indicated, MW mirrors reflecting the incident MW back to the corrugated waveguide are made of 10 nm of gold (to prevent oxidation) deposited on 1-μm deposited layer of aluminum on a 500-μm-thick silicon wafer.

IV. Description of Sample Holders

The six functional parts for different sample types are described individually with HF-ESR measurements.

A. Simple Sample Holder (SSH)

SSH has the simplest functional part (see Fig. 4). It is used for powder samples pressed into pellets of a diameter of 5 mm and a thickness of (1–3) mm, or other solid materials (wafers or crystals) placed directly onto the mirror with the maximum dimension of a cube with a 3.2-mm edge in order to fit into a 5-mm diameter. The SSH functional part is manufactured from PEEK and is equipped with a 5-mm-diameter smooth-wall cylindrical waveguide and a mirror at the bottom. This part is screwed into the body during the measurement, where the corresponding waveguides are aligned with a minimal gap. The simple construction results in the holder with the lowest attenuation of the MW (double pass) 1.4 dB (2.6 dB) at 430 GHz (average attenuation between 260 and 500 GHz) (see Fig. 3 and supplementary information). Moreover, the holder's advantage is a large modulation coil, which gives the best current to field conversion: 1.4 mA/G, a useful feature when recording broad ESR lines where large modulation amplitude B_1 is preferable. At the bottom of Fig. 4, we show an RS ESR measurement on LiPc. By sweeping very fast through the resonance, the oscillations ("wiggles") start to appear in the measured spectrum. These wiggles contain information about T_2 relaxation time and can be simulated by Bloch equations [29], [30].

B. Liquid Sample Holder (LSH)

LSH designed to study liquids or air-sensitive samples has a similar design to SSH with a few adaptations to the functional part, such as a viton o-ring and a sapphire window with a nut placed on top. A nut (PEEK) seals the sample cell upon screwing it into a thread on the top of the functional part

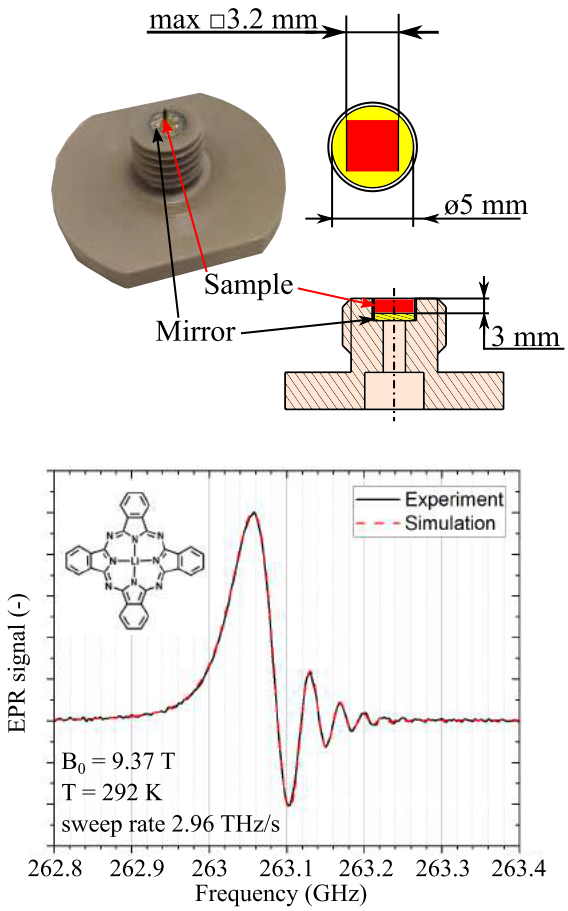

Fig. 4. (Top) Photograph and drawings of the SSH functional part. A sample in the form of a crystal or a pressed powder pellet is fixed onto the mirror by an ESR silent vacuum grease inside a 5-mm-diameter waveguide. The maximum size of the crystal that can be loaded into the SSH is a cube with a 3.2-mm edge. (Bottom) RS ESR spectrum obtained for an LiPC single-crystal sample (1.00 mm × 0.15 mm × 0.15 mm) at 292 K and 420.41 GHz with LiPc molecular structure in the inset. The sweep time was 0.02 ms. A record of spectra was made by the fast acquisition card ADQ7DC (Teledyne Technologies Inc., Thousand Oaks, USA), 10 GSamples/s and 10 × 100 000 averages an overall time of 20 s.

(see Fig. 5). The hermetically sealed cell can hold volatile liquids in a vacuum environment for weeks. Since our system also operates in the FDMR regime, the studied solution is placed directly on the surface of the mirror (located at the bottom of the sample cell), where the magnetic field component B_1 of the MW has its maximum amplitude [41]. The functional part can be manufactured with a groove of different depths for solvents with higher or smaller dielectric losses to get the best possible SH performance [50]. The attenuation of the MW is 2.2 dB (4.7 dB) at 430 GHz (average attenuation between 325 and 500 GHz) in an empty LSH. Apart from the 1-mm thick sapphire window in the MW pathway, the LSH and SSH have a similar design and therefore similar attenuation figures. The data presented in Fig. 5 display the high-frequency measurements of 1 mM ^{14}N-TEMPOL dissolved in acetone. We discovered experimentally that a 4-mm deep groove with 40 μL of solution provides a good ESR signal. FDMR measurements of liquids at frequencies above 300 GHz are unique worldwide. In future, we want to expand this measurement by acquiring T_2 relaxation time via

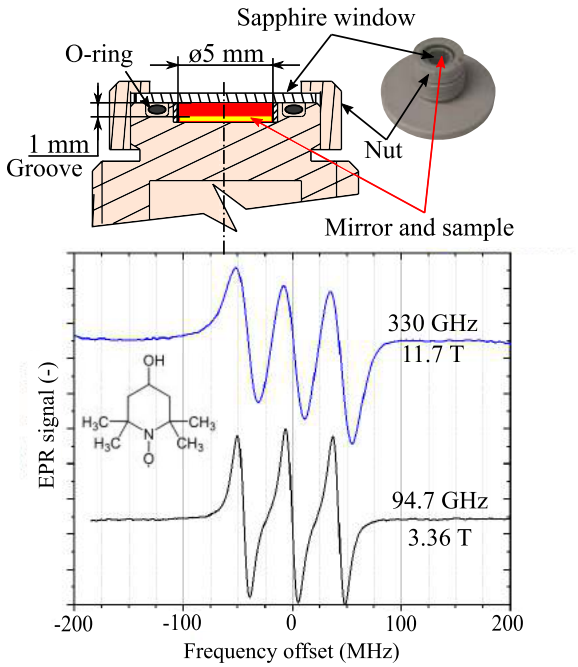

Fig. 5. (Top) Photograph and drawings of the liquid SH's functional part. The liquid sample is hermetically sealed in a cell with the o-ring and a 1-mm-thick sapphire window. The functional part can be manufactured with a different groove deepness according to the solvent needed for the measurements. (Bottom) FDMR measurement of 1 mM of ^{14}N-TEMPOL in acetone at 330 and 94.7 GHz at 300 K. The sweep time was 500 ms, with a field modulation of 6 G at 41 kHz. The final spectra is the average of 64 measurements acquired by MFLI 500-kHz lock-in amplifier (Zurich Instruments Ltd., Zurich, Switzerland).

RS [see Fig. 4 (bottom)], which would boost Dynamic Nuclear Polarization development [14], [51]–[53].

C. Rotator Sample Holder (RSH)

RSH is designed to rotate samples such as single crystals or thin films in the magnetic field during the HF-ESR measurements. The information extracted from those measurements can provide detailed information about the anisotropy of magnetic interactions in paramagnetic materials or solid-state phenomena as cyclotron resonances in conducting materials [54]–[58].

The functional part consists of several cylindrical parts with holes providing a steady flow of helium around the sample for faster cooling downtime. The top rotary base with the leading pin has one degree of freedom and can rotate by 360°. Three leading pins in the functional part and the guiding grooves in the body guarantee the correct alignment of the electrical contacts, while the rotary base of the functional part allows transference of the rotary motion of the screw to a linear motion. The unique position of the three leading pins ensures only one possible loading position (see Fig. 6). The RSH's functional part provides 11 contacts, five of which are used for the piezo-rotator (2) and built-in encoder (3), while the remaining contacts are for the T-sensor and an eventual heater or field sensor. A crystal sample is located on the sapphire rod (Crytur a.s., Turnov, Czech Republic), which is connected directly to a piezo-rotator (ANRv51/RES/LT, Attocube systems AG, Haar, Germany). It can work at temperatures below 4 K, in UHV

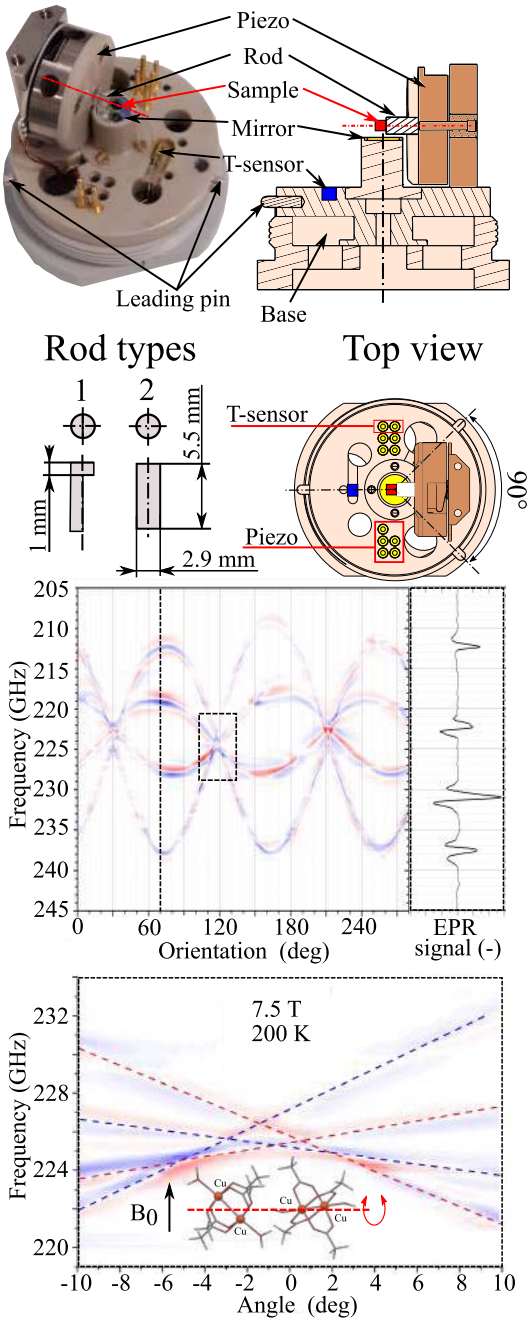

Fig. 6. (Top) Picture and drawings of the RSH functional part, rod types, and top view. A sample is glued on the sapphire shaft using an ESR silent vacuum grease, eicosan, or epoxy. Depending on the experiment, two types of rods are available. The first, with a semi-cylindrical shape, is mainly used for studying thin-layered materials (the maximal thickness of the layer is 1.2 mm). The second, with a cylindrical shape, is used for studying crystals with a maximal size of a cube with a 2.5-mm edge. The necessary electrical connection for the piezo and T-sensor is connected automatically during the screwing of the functional part into the SH's body. The leading pins with unique orientation prevent the unwanted exchange of contacts. (Middle) The rotation map of copper acetate from 0° to 280° at a magnetic field of 7.5 T. The detail on the right displays a spectrum of one frequency sweep at 70°. The acquisition time of each FDMR spectrum is 16 s, and the map was measured in 103 min. (Bottom) A detailed map at the crossing of the ESR lines with an angular step of 0.1°.

and high magnetic fields. Moreover, it has a built-in encoder allowing measurements with a very fine resolution of 0.006° [see Fig. 6 (bottom)]. The direct connection of the sapphire

rods minimizes errors caused by the rotation. The mirror is placed 2 mm under the axis of the sapphire rod. A magnetic field sensor can be placed under the mirror. So far, we have designed and manufactured two sapphire rods. One with a semicylindrical shape that offers the possibility of rotation and measurements of thin films or wafers. The second rod has a cylindrical shape that enables measurements of samples with a maximal cubic size with an edge of up to 2.5 mm. To increase MW propagation, the waveguide is prolonged down to the mirror with a cutout only for the sapphire rods (see Fig. 3). However, due to its complex structure, it has the largest return losses out of all SHs, at 430 GHz (average attenuation between 260 and 500 GHz), the return losses are 8 dB (9.1 dB) with the semicylindrical sapphire rod.

The middle and bottom of Fig. 6 displays FDMR rotation maps for a single crystal of copper acetate monohydrate $[Cu(CH_3COO)_2 \cdot H_2O]$. The four ESR signals observed at a single field/frequency correspond to the MW absorption by two rotated molecules in the lattice of this compound. The 0–280° map was obtained by performing automated FDMR measurements and simultaneously rotating the crystal by a 1° step, whereas the detailed map in the range −10°–10° has a 0.1° step. This methodology with FDMR decreases measurement time from days to hours when compared to a field-domain measurement, and still the spectrum at a single orientation can be extracted from the map.

D. Chip Sample Holder (ChSH)

ChSH allows characterization of electrical/electronic devices under MW irradiation or to perform magneto-transport measurements [3]. The functional part contains 20 connectors, 16 of which host a chip expander, while the other four connect the T-sensor and the heater. The chip expander is a small printed circuit board (PCB) with 16 gold deposited holes and contacts, prepared for wire-bonding of samples [3]. The maximal sample size which can be wire bonded is 8 mm × 8 mm. A small mismatch fit between the electrical connectors and the chip expander's holes guarantees tension for a reliable connection. Any device prepared and wire-bonded to the chip expander can be easily loaded with minimal user interaction (see Fig. 7). A sapphire heat sink is placed under the chip expander in order to dissipate the heat effectively to the sample. The heat sink has to be non-conductive to prevent shortcuts between contacts and eddy currents produced by the modulated magnetic field. Therefore, a sapphire plate was chosen for its non-conductance and good thermal conductivity at low temperatures [59]. The T-sensor and the heater are glued to the bottom side of the sapphire plate, which allows precise temperature control of the sample with a stability in the order of 10 mK. Furthermore, the effective helium cooling is provided by holes in the functional part. Similar to the RSH, three leading pins in the functional part and the guiding grooves in the body guarantee the correct alignment of the electrical contacts, while the rotary base of the functional part allows the transference of the rotary motion of the screw to a linear motion. After screwing the functional part, there is a gap between the sample and

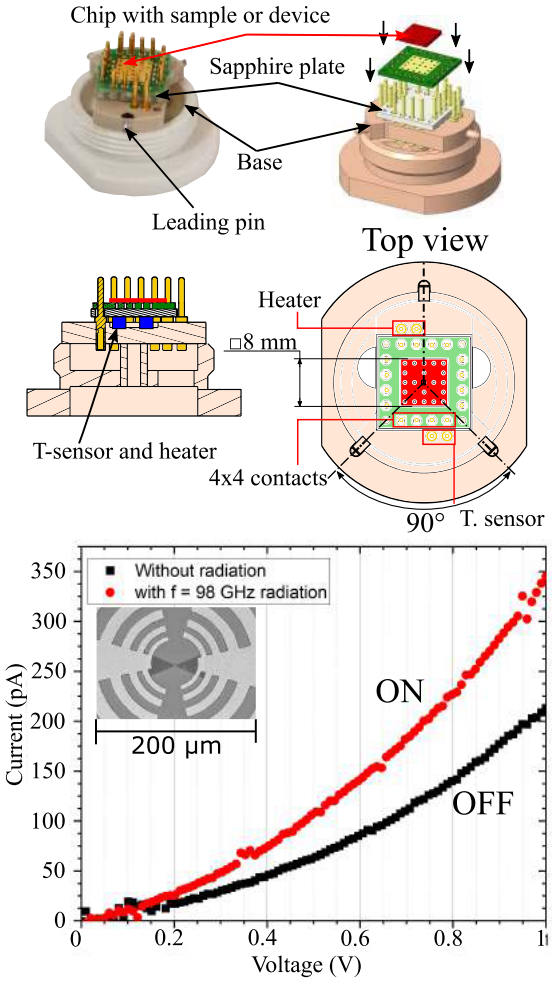

Fig. 7. (Top) Picture and drawings of the ChSH functional part. The T-sensor and the heater are under the sapphire plate, which works as a heat buffer. The sample is glued onto the chip that is inserted into the male connectors of the functional part. The interspace between the contacts is slightly bigger than the interspace between the holes in the chip, ensuring good electrical contact at any temperature. (Bottom) Measurements of a graphene bolometer's I/V curves with (ON) and without (OFF) MW irradiation at 15 K. The design of the bolometer is in the inset of the plot.

the waveguide to avoid the sample being touched by wire bonds, resulting a backward reflected ESR measurements with a 5.9 dB (5.8 dB) loss at 430 GHz (average attenuation between 260 and 500 GHz).

Fig. 7 shows an example of the I/V characteristics of a graphene bolometer [60]. We tested the bolometer response to microwave radiation at 98 GHz (red line). The I/V response with (ON) and without (OFF) MW irradiation was measured with a zero external magnetic field applied. The shift in curves is caused by MW irradiation and changes in the bolometer resistance. This represents the characteristic behavior of the bolometer [60].

E. Carousel Sample Holder (CSH)

CSH was designed to load up to six samples in individual cells simultaneously inside a side-loaded rotary platform in the functional part (see Fig. 8). The process of changing the sample directly inside the magnet significantly reduces the spectrometer usage time. The time-saving feature is especially

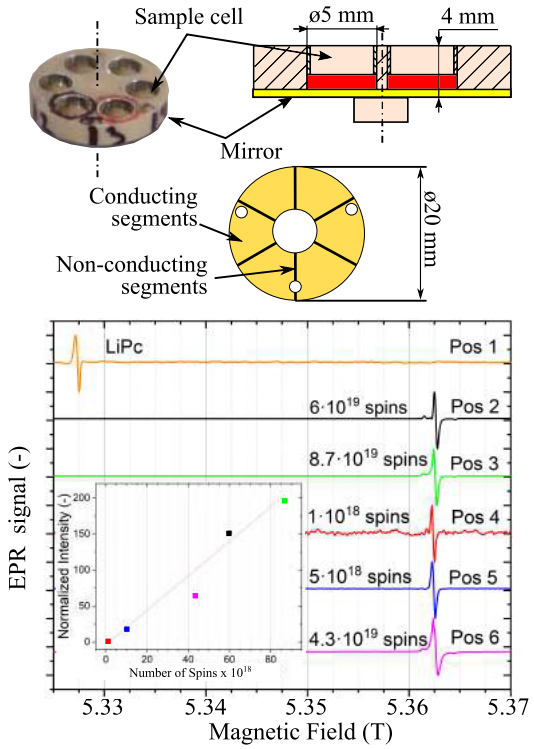

Fig. 8. (Top) Picture and drawings of the six-cell rotary platform of the CSH. Samples are glued on the rotary platform's mirror by an ESR-silent vacuum grease. The mirror is divided into conducting and non-conducting segments, reducing the eddy currents created by the modulation coil. (Bottom) CW-ESR measurements using the different cells at room temperature loaded at once (five BDPA samples with different concentrations and one reference LiPc sample, which serves for spectrometer optimization). The magnetic field sweep was 0.5 mT/s with field modulation of 10.1 kHz and amplitude 30 G. The measurements are normalized to the intensity of the weakest spectrum (red). The inset shows the plot of the normalized intensities for each sample against their number of spins. Change among different samples takes a few seconds with the SH placed inside the magnet VTI.

significant for low-temperature experiments. In the presented spectrometer, a typical time to cool down the SSH from 300 K to a stable 4 K is about 6 h. To exchange samples, the cryostat has to be warmed up before the ESR probe can be unloaded. This process takes an additional 1 h. With the carousel implementation, the user can switch between six samples directly in the cryostat without unloading the probe, thus saving up to 30 h overall. Moreover, one of the six cells can be filled with a well-known reference sample for the system optimization/calibration. Additionally, CSH is the best possible solution for future quantitative high-field ESR applications, because the samples are switched directly inside the SH without changing the MW coupling. Each sample cell is 5 mm in diameter and 4-mm in depth. For better MW propagation, the cells' walls are made from an aluminum smooth-wall waveguide, as in the corresponding body.

The reflection in the CSH is achieved by a large home-made mirror shared by all cells cut from a silicon wafer coated by aluminum and gold in the same manner as previously mentioned. One large shared mirror minimizes the differences in the MW coupling between cells due to reflecting differences (see supplementary information). The precise position of the sample cells with respect to the body's waveguide is achieved by a piezo step motor (PiezoMotor Uppsala AB, Uppsala, Sweden) located outside of the cryostat (see Fig. 2). It is connected through a shaft to a gear mechanism in the body (see Fig. 3) and with the rotating platform (functional part). With a 0.01° motor step and a gear mechanism (gears ratio 1/5) made from brass, we have the theoretical step precision of 0.002°. However, due to the large temperature operation range (4–400 K), all movable parts must have enough space, or a Teflon bearing, to avoid friction and freezing at low temperatures. With the temperature decrease, Teflon shrinks more than PEEK or metals, providing clearance for rotation, but at the cost of the rotation accuracy [61]. To ensure proper m.w. coupling between the body and functional part, the positioning system is composed of a potentiometer/encoder ring (a graphite/silver thick film on the ceramic substrate, made by SEANT Technology s.r.o., Brno, Czech Republic) glued to the bottom of the SH's body, and a slider made of phosphor–bronze mounted directly to a bigger gear whose axis is parallel to the encoder axis and the sample functional part axis (see Fig. 3). The encoder ring resistance is 22 kΩ at room temperature, and 24 kΩ at 4 K. The feedback control of the SH is performed automatically via a script included in the home-built LabVIEW software of the FRaSCAN spectrometer. It measures the resistance at the actual position and resistance of the whole ring by the application of a constant current value. The ratio between these two values does not change with the temperature. With this system, we can change the sample cell within our temperature working range with the precision of 0.05° and ensure good MW coupling. The MW attenuation in the CSH is 2.2 dB (2.1 dB) at 430 GHz (average attenuation between 260 and 500 GHz). The worse results of the MW attenuation compared with the SSH is due to a small gap (≈0.2) between the waveguide in the connector part and the platform, and waveguide mismatches.

Preliminary results of our quantitative ESR measurements are shown in Fig. 8. The CSH was loaded by five differently concentrated α,γ-bisdiphenylene-β-phenylallyl (BDPA) samples and one LiPc reference sample. The intensity of the BDPA signal from each sample follows its concentration (see the inset in Fig. 8).

F. Vacuum Sample Holder (VSH)

VSH in combination with a mobile UHV suitcase (see supplementary information) allows the study of air-sensitive structures prepared in a UHV chamber. It is based on an Omicron plate (Scienta Omicron GmbH, Taunusstein Germany) for transporting air-sensitive samples which are often manufactured and studied in UHV systems (see Fig. 9). A sample in the form of a deposited layer on a single crystal of copper, gold, iridium, and so on (Structure Probe Inc., West Chester, USA) or on a wafer it is fixed to the Omicron plate and side loaded into the VSH. A crystal or a wafer serves as the mirror for ESR measurements. The MW attenuation of the holder is 6 dB (7.2 dB) at 430 GHz (average attenuation between 325 and 500 GHz). However, the size of the crystal and the metallic plate decreases the efficiency of the modulation coil (see Fig. 3). Thanks to the VSH, HF-ESR measurements are possible in addition to the X-ray photoelectron spectroscopy (XPS), scanning

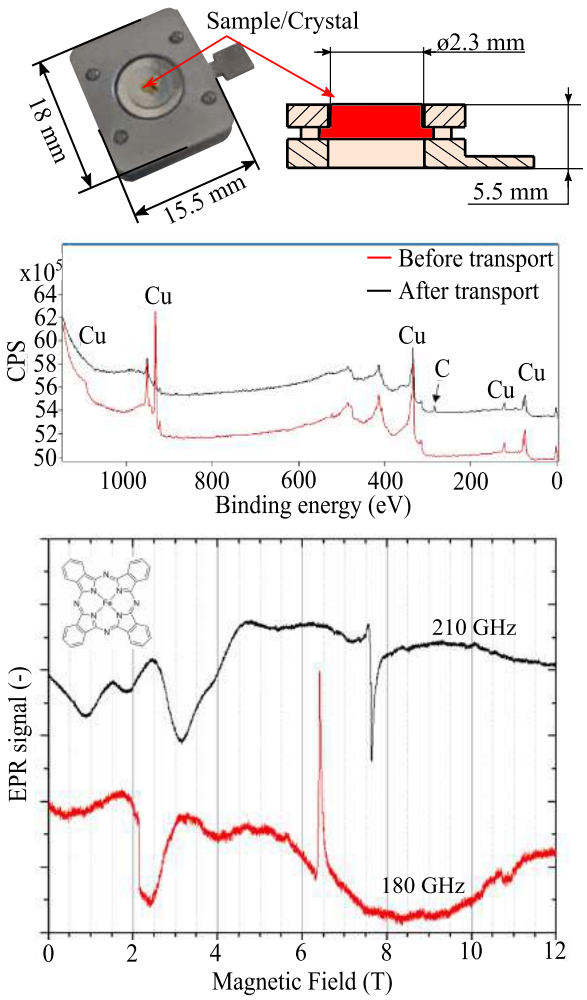

Fig. 9. (Top) Picture and drawings of the VSH's functional part. The different crystals made of aluminum, gold, silver, or copper can be fixed between two Omicron plates, and the studied structure is then deposited on top of it. (Middle) XPS spectra of a crystalline copper sample before and after the transport between the HF-ESR spectrometer and the XPS chamber. Carbon atoms were the only detectable impurities on the surface. (Bottom) The CW-ESR measurements of the Fe–Pt pressed-powder pellet placed on the functional part.

tunneling microscopy (STM), low-energy electron diffraction (LEED), and other techniques often used in nano-fabrication clusters [62]–[64].

The proof-of-concept ESR measurements were done with a pressed-pellet of iron(II) phthalocyanine (FePc) placed on the Omicron plate [see Fig. 9 (bottom)]. To check the contamination during the transfer, the test transfer was done with a clean copper crystal. After the sample was transferred back into the UHV cluster, XPS spectra were acquired and compared with the XPS spectra before transportation [see Fig. 9 (middle)], resulting in minor carbon contamination.

V. Samples

A. 4-Hydroxy-2,2,6,6-Tetramethylpiperidine 1-Oxyl (TEMPOL)

The TEMPOL was bought from Sigma Aldrich and dissolved in acetone with a concentration of 1 mM. The spectra shown in Fig. 5 were recorded without sample degassing.

B. Copper Acetate Monohydrate

Single crystals of the dimeric copper acetate monohydrate ($[Cu(CH_3COO)_2 \cdot H_2O]$) were obtained as follows: copper(II) acetate (10 g, 50 mmol) was dissolved in 50 mL of 70 °C water and stirred until a supersaturated solution was obtained. A drop of concentrated acetic acid was added during stirring to prevent reduction to Cu(I), which was observed otherwise. The solution was filtered with a 0.2 μm micropore filter and kept under a constant temperature of 40 °C in an oil bath in order to decrease volume and initiate crystallization. Crystals of about 2 mm^2 were grown after two days and selected for the ESR measurement tests in this work. The selected crystal was randomly oriented in the RSH, which is prepared by Lubomír Havlíček (CEITEC, BUT, Brno, Czech Republic).

C. Graphene-Based Bolometer

A bolometer fabricated from epitaxial graphene on silicon carbide. These bolometers utilized a graphene quantum dot to produce a temperature-dependent resistance [60]. Due to quantum confinement effects, thermal activation is required for conduction across the dot, producing a highly responsive broadband detector at low temperatures. This nanostructured graphene device was used to measure radiation intensity at frequencies between 10 GHz and 1 THz.

D. Lithium Phthalocyanine (LiPc)

Lithium phthalocyanine in microcrystalline form was prepared electrochemically following a procedure described in the literature [65], [66]. A sample in the form of a crystal was obtained from Mark Tseylin (West Virginia University, Morgantown, WV, USA). The sharp single crystal was chosen and glued onto mirror using vacuum grease.

E. α, γ -Bisdiphenylene-β-Phenylallyl (BDPA)

The BDPA was bought from Sigma Aldrich and dissolved in toluene together with polystyrene (bought from Sigma Aldrich) to the desired concentration [see Fig. 8 (bottom)]. After dissolving, the final mixture was dropped onto the mirror, where the toluene evaporated overnight, creating a film of polystyrene with BDPA inside its matrix.

F. Iron Phthalocyanine (FePc)

The FePc in the crystal form was bought from Sigma Aldrich. Fifteen milligrams of the sample with 5 mg of icosane was ground into powder and pressed into a pellet.

VI. Conclusion

This article introduces a family of sample holders based on a fast loading flange for sub-THz ESR spectroscopy. The presented concept of sample holders significantly improves our measurement time and user-friendliness during the preparation of the measurements. Moreover, we present the system of sample holders that can expand the capabilities of any resonance-free ESR spectrometer. The materials for sample holders were chosen carefully, considering thermal and

mechanical stability at room temperature as well at liquid helium temperatures. The article goes from a basic description of each SH and a demonstration of its functionality through illustrative measurements. The result of this work significantly broadens the measurement capabilities and applicability of our FRaSCAN-ESR spectrometer, enabling an extended range of materials to be studied either in the field domain or in the frequency domain, and providing a reliable and comprehensive investigation of materials. Furthermore, the fast-loading flange can be used for a variety of different sample holders in the future.

ACKNOWLEDGMENT

The authors would like to thank all members of MOTeS CEITEC group for fruitfull discussion during the design of the SHs, especially they would also like to thank Ing. Tomáš Martínek for help with first sketch of SHs, Dr. Jakub Hrubý and Lubomír Havlíček for assistance in bolometer measurements and in sample preparations, respectively. Prof. Paola Barbara and Dr. Luke St. Marie (Georgetown University, Washington, DC, USA) for providing the graphene-based bolometers. Prof. Mark Tseytlin (West Virginia University, Morgantown, WV, USA) for giving them LiPc single crystals. Prof. Jan Čechal and his group (CEITEC, BUT, Brno, Czech Republic) for help in setting up measurements using vacuum SH. Moreover, Rohde&Schwartz Czech Republic for providing Vector Network Analyser used in the measurements of microwave losses.

REFERENCES

[1] E. Zavoisky, "The paramagnetic absorption of a solution in parallel fields," *J. Phys.*, vol. 3, pp. 211–216, Sep. 2011.

[2] J. R. Biller and J. E. McPeak, "EPR everywhere," *Appl. Magn. Reson.*, vol. 52, no. 8, pp. 1113–1139, Jan. 2021.

[3] D. Bloos *et al.*, "Contactless millimeter wave method for quality assessment of large area graphene," *2D Mater.*, vol. 6, no. 3, May 2019, Art. no. 035028.

[4] P. Schlottmann, "Theory of electron spin resonance in ferromagnetically correlated heavy fermion compounds," *Magnetochemistry*, vol. 4, no. 2, p. 27, Jun. 2018.

[5] D. Gatteschi, R. Sessoli, and J. Villain, *Molecular Nanomagnets*, vol. 9780198567530. London, U.K.: Oxford Univ. Press, Sep. 2007.

[6] D. Abdullin and O. Schiemann, "Pulsed dipolar EPR spectroscopy and metal ions: Methodology and biological applications," *ChemPlusChem*, vol. 85, no. 2, pp. 353–372, Feb. 2020.

[7] P. Neugebauer, M. Orlita, C. Faugeras, A.-L. Barra, and M. Potemski, "How perfect can graphene be?" *Phys. Rev. Lett.*, vol. 103, no. 13, Sep. 2009, Art. no. 136403.

[8] G. Wolfowicz and J. Morton, "Pulse techniques for quantum information processing," *eMagRes*, vol. 5, no. 4, pp. 1515–1528, 2016.

[9] C. Godfrin *et al.*, "Operating quantum states in single magnetic molecules: Implementation of Grover's quantum algorithm," *Phys. Rev. Lett.*, vol. 119, no. 18, Nov. 2017, Art. no. 187702.

[10] I. D. Sahu and G. A. Lorigan, "Biophysical EPR studies applied to membrane proteins," *J. Phys. Chem. Biophys.*, vol. 5, no. 6, p. 188, 2015.

[11] I. D. Sahu and G. A. Lorigan, "Site-directed spin labeling EPR for studying membrane proteins," *BioMed Res. Int.*, vol. 2018, pp. 1–13, Jan. 2018.

[12] O. Schiemann and T. F. Prisner, "Long-range distance determinations in biomacromolecules by EPR spectroscopy," *Quart. Rev. Biophys.*, vol. 40, no. 1, pp. 1–53, Feb. 2007.

[13] J. P. Klare and H.-J. Steinhoff, "Spin labeling EPR," *Photosynthesis Res.*, vol. 102, nos. 2–3, pp. 377–390, Dec. 2009.

[14] A. Marko, A. Sojka, O. Laguta, and P. Neugebauer, "Simulation of nitrogen nuclear spin magnetization of liquid solved nitroxides," *Phys. Chem. Chem. Phys.*, vol. 23, no. 32, pp. 17310–17322, Aug. 2021.

[15] M. M. Roessler and E. Salvadori, "Principles and applications of EPR spectroscopy in the chemical sciences," *Chem. Soc. Rev.*, vol. 47, no. 8, pp. 2534–2553, 2018.

[16] M. Drescher and G. Jeschke, *EPR Spectroscopy* (Topics in Current Chemistry), vol. 321. Berlin, Germany: Springer, 2012.

[17] E. Coronado, "Molecular magnetism: From chemical design to spin control in molecules, materials and devices," *Nature Rev. Mater.*, vol. 5, no. 2, pp. 87–104, Feb. 2020.

[18] D. Hanneke, S. Fogwell, and G. Gabrielse, "New measurement of the electron magnetic moment and the fine structure constant," *Phys. Rev. Lett.*, vol. 100, no. 12, Mar. 2008, Art. no. 120801.

[19] M. Rohrer, O. Brügmann, B. Kinzer, and T. F. Prisner, "High-field/high-frequency EPR spectrometer operating in pulsed and continuous-wave mode at 180 GHz," *Appl. Magn. Reson.*, vol. 21, nos. 3–4, pp. 257–274, Dec. 2001.

[20] A. Gaita-Ariño, F. Luis, S. Hill, and E. Coronado, "Molecular spins for quantum computation," *Nature Chem.*, vol. 11, no. 4, pp. 301–309, Mar. 2019.

[21] F. Tuna, "Reaction: Molecular spins as qubits," *Chem*, vol. 6, no. 4, pp. 799–800, Apr. 2020.

[22] S. Realista *et al.*, "A Mn(III) single ion magnet with tridentate Schiff-base ligands," *Dalton Trans.*, vol. 45, no. 31, pp. 12301–12307, 2016.

[23] I. Nemec, R. Herchel, M. Kern, P. Neugebauer, J. Van Slageren, and Z. Trávníček, "Magnetic anisotropy and field-induced slow relaxation of magnetization in tetracoordinate Co^{II} compound $[Co(CH_3\text{-im})_2Cl_2]$," *Materials*, vol. 10, no. 3, p. 249, 2017.

[24] Y.-Y. Zhu *et al.*, "The solvent effect in an axially symmetric Fe_4^{III} single-molecule magnet," *Chem. Commun.*, vol. 50, no. 95, pp. 15090–15093, 2014.

[25] T. K. Prasad *et al.*, "Magnetic and optical bistability in tetrairon(III) single molecule magnets functionalized with azobenzene groups," *Dalton Trans.*, vol. 41, no. 27, pp. 8368–8378, 2012.

[26] J. Telser, A. Ozarowski, and J. Krzystek, "High-frequency and-field electron paramagnetic resonance of transition metal ion (d block) coordination complexes," *Electron Paramagn. Reson.*, vol. 23, no. 1, pp. 209–263, Nov. 2012.

[27] S. Misra, *Multifrequency Electron Paramagnetic Resonance: Theory and Applications*, Wiley-VCH, Ed., 1st Ed. Hoboken, New Jersey, Apr. 2011.

[28] C. Danieli *et al.*, "A novel class of tetrairon(III) single-molecule magnets with graphene-binding groups," *Polyhedron*, vol. 28, nos. 9–10, pp. 2029–2035, Jun. 2009.

[29] A. Sojka, M. Šedivý, O. Laguta, A. Marko, V. Santana, and P. Neugebauer, "High-frequency EPR: Current state and perspectives," *Electron Paramagn. Reson.*, vol. 27, pp. 214–252, Nov. 2021.

[30] O. Laguta, M. Tuček, J. van Slageren, and P. Neugebauer, "Multi-frequency rapid-scan HFEPR," *J. Magn. Reson.*, vol. 296, pp. 138–142, Nov. 2018.

[31] V. A. Soltamov *et al.*, "Electron nuclear interactions in spin-3/2 color centers in silicon carbide: A high-field pulse EPR and ENDOR study," *Phys. Rev. B, Condens. Matter*, vol. 104, no. 12, Sep. 2021, Art. no. 125205.

[32] K. Möbius and A. Savitsky, *High-Field EPR Spectroscopy on Proteins and Their Model Systems*. London, U.K.: Royal Society of Chemistry, Dec. 2008.

[33] K. Möbius, A. Schnegg, M. Plato, M. R. Fuchs, and A. Savitsky, "High-field EPR spectroscopy on transfer proteins in biological action," *Acta Phys. Polonica A*, vol. 108, no. 2, pp. 215–234, Aug. 2005.

[34] P. Neugebauer *et al.*, "Ultra-broadband EPR spectroscopy in field and frequency domains," *Phys. Chem. Chem. Phys.*, vol. 20, no. 22, pp. 15528–15534, 2018.

[35] A. Engalytcheff, M. Kolberg, A.-L. Barra, K. Kristoffer Andersson, and B. Tilquin, "The use of multi-frequency EPR techniques to identify the radicals produced in irradiated β-blockers," *Free Radical Res.*, vol. 38, no. 1, pp. 59–66, Jan. 2004.

[36] P. Neugebauer and A.-L. Barra, "New cavity design for broad-band quasi-optical HF-EPR spectroscopy," *Appl. Magn. Reson.*, vol. 37, nos. 1–4, pp. 833–843, Nov. 2009.

[37] E. Ohmichi, Y. Shoji, H. Takahashi, and H. Ohta, "Frequency-domain electron spin resonance spectroscopy using continuously frequency-tunable terahertz photomixers," *Appl. Phys. Lett.*, vol. 119, no. 16, Oct. 2021, Art. no. 162404.

[38] J. van Slageren *et al.*, "Frequency-domain magnetic resonance spectroscopy of molecular magnetic materials," *Phys. Chem. Chem. Phys.*, vol. 5, pp. 3837–3843, Sep. 2003.
[39] A. Schnegg, *Very-High-Frequency EPR*. Hoboken, NJ, USA: Wiley, 2017, pp. 115–132.
[40] J. van Tol, L.-C. Brunel, and R. J. Wylde, "A quasioptical transient electron spin resonance spectrometer operating at 120 and 240 GHz," *Rev. Sci. Instrum.*, vol. 76, no. 7, Jul. 2005, Art. no. 074101.
[41] L. Song *et al.*, "Toward increased concentration sensitivity for continuous wave EPR investigations of spin-labeled biological macromolecules at high fields," *J. Magn. Reson.*, vol. 265, pp. 188–196, Apr. 2016.
[42] J. P. Barnes and J. H. Freed, "Aqueous sample holders for high-frequency electron spin resonance," *Rev. Sci. Instrum.*, vol. 68, no. 7, pp. 2838–2846, Jul. 1997.
[43] S. Kimura *et al.*, "Submillimeter wave ESR measurements of metamagnetic $Y_2Cu_2O_5$," *Int. J. Infr. Millim. Waves*, vol. 17, no. 5, pp. 833–841, May 1996.
[44] G. Eaton and S. Eaton, "Rapid-scan electron paramagnetic resonance," *eMagRes*, vol. 5, no. 4, pp. 1529–1542, Dec. 2016.
[45] J. Dadok and R. F. Sprecher, "Correlation NNW spectroscopy," *J. Magn. Reson.*, vol. 13, no. 2, pp. 243–248, Feb. 1974.
[46] J. W. Stoner, D. Szymanski, S. S. Eaton, R. W. Quine, G. A. Rinard, and G. R. Eaton, "Direct-detected rapid-scan EPR at 250 MHz," *J. Magn. Reson.*, vol. 170, no. 1, pp. 127–135, Sep. 2004.
[47] O. Laguta, A. Sojka, A. Marko, and P. Neugebauer, "Rapid scan ESR: A versatile tool for the spin relaxation studies at (sub)THz frequencies," *Appl. Phys. Lett.*, vol. 120, no. 12, Mar. 2022, Art. no. 120502.
[48] G. Smith and P. C. Riedi, "Progress in high field EPR," in *Electron Paramagnetic Resonance*, The Royal Society Of Chemistry. London, U.K.: 2000, pp. 164–204.
[49] J. M. Gaitonde and M. V. Lowson, "Low-temperature thermal expansion of PEEK, HTA and some of their composites reinforced with carbon fibres," *Compos. Sci. Technol.*, vol. 40, no. 1, pp. 69–85, Jan. 1991.
[50] Y. E. Nesmelov, A. Gopinath, and D. D. Thomas, "Aqueous sample in an EPR cavity: Sensitivity considerations," *J. Magn. Reson.*, vol. 167, no. 1, pp. 138–146, Mar. 2004.
[51] P. Neugebauer, J. G. Krummenacker, V. P. Denysenkov, G. Parigi, C. Luchinat, and T. F. Prisner, "Liquid state DNP of water at 9.2 T: An experimental access to saturation," *Phys. Chem. Chem. Phys.*, vol. 15, no. 16, pp. 6049–6056, 2013.
[52] P. Neugebauer *et al.*, "High-field liquid state NMR hyperpolarization: A combined DNP/NMRD approach," *Phys. Chem. Chem. Phys.*, vol. 16, no. 35, pp. 18781–18787, 2014.
[53] S. E. Küçük, P. Neugebauer, T. F. Prisner, and D. Sezer, "Molecular simulations for dynamic nuclear polarization in liquids: A case study of TEMPOL in acetone and DMSO," *Phys. Chem. Chem. Phys.*, vol. 17, no. 9, pp. 6618–6628, 2015.
[54] F. El Hallak, P. Neugebauer, A.-L. Barra, J. van Slageren, M. Dressel, and A. Cornia, "Torque-detected ESR of a tetrairon(III) single molecule magnet," *J. Magn. Reson.*, vol. 223, pp. 55–60, Oct. 2012.
[55] R. P. Sartoris, V. T. Santana, E. Freire, R. F. Baggio, O. R. Nascimento, and R. Calvo, "Exchange couplings and quantum phases in two dissimilar arrays of similar copper dinuclear units," *Dalton Trans.*, vol. 49, no. 16, pp. 5228–5240, Apr. 2020.
[56] T. Yamane *et al.*, "Analyses of sizable ZFS and magnetic tensors of high spin metallocomplexes," *Phys. Chem. Chem. Phys.*, vol. 19, no. 36, pp. 24769–24791, 2017.
[57] M. Šimėnas *et al.*, "Single crystal electron paramagnetic resonance of dimethylammonium and ammonium hybrid formate frameworks: Influence of external electric field," *J. Phys. Chem. C*, vol. 121, no. 30, pp. 16533–16540, Aug. 2017.
[58] V. T. Santana *et al.*, "Magnetic-field-tuned phase transition of a molecular material from the isolated-spin to the coupled-spin regime," *Phys. Chem. Chem. Phys.*, vol. 21, no. 8, pp. 4394–4407, 2019.
[59] J. Ekin, *Experimental Techniques for Low-Temperature Measurements: Cryostat Design, Material Properties and Superconductor Critical-Current Testing*. London, U.K.: Oxford Univ. Press, Oct. 2006.
[60] L. S. Marie *et al.*, "Nanostructured graphene for nanoscale electron paramagnetic resonance spectroscopy," *J. Phys., Mater.*, vol. 3, no. 1, Jan. 2020, Art. no. 014013.
[61] C. A. Swenson, "Mechanical properties of Teflon at low temperatures," *Rev. Sci. Instrum.*, vol. 25, no. 8, p. 834, Dec. 2004.
[62] L. Kormoš, P. Procházka, A. O. Makoveev, and J. Čechal, "Complex k-uniform tilings by a simple bitopic precursor self-assembled on Ag(001) surface," *Nature Commun.*, vol. 11, no. 1, pp. 1–6, Apr. 2020.
[63] J. Hrubý *et al.*, "A graphene-based hybrid material with quantum bits prepared by the double Langmuir–Schaefer method," *RSC Adv.*, vol. 9, no. 42, pp. 24066–24073, 2019.
[64] F. Ciccullo *et al.*, "Thin film properties and stability of a potential molecular quantum bit based on copper(II)," *J. Mater. Chem. C*, vol. 6, no. 30, pp. 8028–8034, 2018.
[65] P. Turek, J.-J. André, A. Giraudeau, and J. Simon, "Preparation and study of a lithium phthalocyanine radical: Optical and magnetic properties," *Chem. Phys. Lett.*, vol. 134, no. 5, pp. 471–476, Mar. 1987.
[66] M. Afeworki *et al.*, "Preparation and EPR studies of lithium phthalocyanine radical as an oxymetric probe," *Free Radical Biol. Med.*, vol. 25, no. 1, pp. 72–78, Jul. 1998.

Antonín Sojka received the bachelor's and master's degrees from the Brno University of Technology, Brno, Czech Republic, in 2016 and 2018, respectively. He is currently pursuing the Ph.D. degree with the Central European Institute of Technology, BUT, under the supervision of Petr Neugebauer in the group Magneto-Optical and Terahertz Spectroscopy (MOTES).

His research interests include the development of high-field broad-frequency ESR for relaxation studies with focus on rapid scan techniques.

Matúš Šedivý received the master's degree in microelectronics from the Brno University of Technology, Brno, Czech Republic, in 2017. He is currently pursuing the Ph.D. degree working in a group of MOTES on development of a Fast Electron Spin Resonance Spectroscopy Measurement System at Terahertz Frequencies.

He focuses on the development of software for automated control of a custom-built HF-ESR spectrometer and upgrade of hardware to expand capabilities of the spectrometer. His research interest is application of ESR to study semiconductors.

Adam Lagiň was born in Považská Bystrica, Slovakia, in 1998. He received the bachelor's degree from the Fundamentals of Mechanical Engineering, Brno University of Technology, Brno, Czech Republic, in 2020. During this time, he resolved the design of onant sample holders for a high-field electron spin resonance spectrometer. His master's studies recently continue at the Institute of Machine and Industrial Design with the research focused on additively manufactured metallic micro-truss lattices and their vibration-dynamical properties.

Andrej Gabriš received the bachelor's degree from the Fundamentals of Mechanical Engineering, Brno University of Technology (BUT), Brno, Czech Republic, in 2020. During this time, he resolved the design of nonresonant sample holders for a high-field electron spin resonance spectrometer at the Central European Institute of Technology, Brno. His master's studies recently continue at the Institute of Machine and Industrial Design, BUT, with the research focused on additively manufactured metallic micro-truss lattices and their vibration-dynamical properties.

Tomáš Láznička received the Ing. degree in applied physics (physical engineering and nanotechnology) from the Brno University of Technology, Brno, Czech Republic, in 2020. He is currently pursuing the Ph.D. degree in the group of Dr. Krzyžánek with the Institute of Scientific Instruments, Czech Academy of Science, Prague, Czech Republic, working on cryo-electron microscopy and microfluidic systems.

He was a Team Member of the Petr Neugebauer's Research MOTES Group, CEITEC, Brno.

Vinicius Tadeu Santana received the Ph.D. degree in applied physics from the University of São Paulo, São Paulo, Brazil, in 2016, working with exchange-coupled molecular compounds using ESR spectroscopy supervised by Prof. O. R. Nascimento.

He is currently a Junior Research Fellow with the Central European Institute of Technology, Brno University of Technology, Brno, Czech Republic, and a Team Member of Prof. P. Neugebauer's Group, working with applications of ESR in molecular spin systems and solid-state magnetic materials.

Oleksii Laguta received the Ph.D. degree in lasers, molecules, atmospheric radiation from the University of Lille, Lille, France, in 2016.

After that, he spent 18 months working on the development of frequency-domain rapid-scan HF-ESR as a Post-Doctoral Research Fellow in the group of Petr Neugebauer (AG van Slageren, Stuttgart University, Stuttgart, Germany). Since 2019, he has been a Junior Researcher with the Central European Institute of Technology, Brno, Czech Republic. Currently, he studies the electron spin dynamics at high magnetic fields using the rapid-scan ESR spectroscopy.

Petr Neugebauer received the Ph.D. degree with Marie Curie fellowship from the Physics of Condensed Matter and Radiation, Grenoble High Magnetic Field Laboratory (GHMFL), Grenoble, France, in 2010.

After his two years post-doctoral stay in the research group of Prof. T. Prisner at the Center for Biomolecular Magnetic Resonance, Goethe University, Frankfurt, Germany, he joined the research group of Prof. J. van Slageren at the University of Stuttgart, Stuttgart, Germany. He is currently the Group Leader and the Founder of the MOTeS group, CEITEC, BUT, Brno, Czech Republic. The group focuses on the development of high-frequency electron spin resonance (HF-ESR) spectroscopy, especially frequency rapid scan above 100 GHz (ERC grant), HF-ESR applications to molecular magnetism, thin films, and molecular materials.